IOP Publishing Phys. Med. Biol. 69 (2024) 205012 https://doi.org/10.1088/1361-6560/ad7fc8

Physics in Medicine & Biology

IPEM Institute of Physics and Engineering in Medicine

OPEN ACCESS

RECEIVED
4 March 2024

REVISED
12 September 2024

ACCEPTED FOR PUBLICATION
25 September 2024

PUBLISHED
8 October 2024

PAPER

Enhancing timing performance of heterostructures with double-sided readout

Fiammetta Pagano[1,2,5,*], **Nicolaus Kratochwil**[1,6], **Carsten Lowis**[1,3], **Woon-Seng Choong**[4], **Marco Paganoni**[1,2], **Marco Pizzichemi**[1,2], **Joshua W Cates**[4] and **Etiennette Auffray**[1]

[1] CERN, Esplanade des Particules 1, 1211 Geneva, Switzerland
[2] University of Milano-Bicocca, Piazza dell'Ateneo Nuovo, 1, 20126 Milan, Italy
[3] FH Aachen University of Applied Sciences, Jülich, Germany
[4] Lawrence Berkeley National Laboratory, Berkeley, CA, United States of America
[5] Now at: Instituto de Instrumentación para Imagen Molecular (I3M), Centro Mixto CSIC—Universitat Politècnica de València, Camino de Vera s/n, 46022 Valencia, Spain
[6] Now at: Department of Biomedical Engineering, University of California, Davis, CA, United States of America
* Author to whom any correspondence should be addressed.

E-mail: fiammetta.pagano@cern.ch

Keywords: time-of-flight PET, coincidence time resolution, heterostructured scintillators, depth of interaction, high-frequency, double-sided readout

Abstract

Objective. Heterostructured scintillators offer a promising solution to balance the sensitivity and timing in TOF-PET detectors. These scintillators utilize alternating layers of materials with complementary properties to optimize performance. However, the layering compromises time resolution due to light transport issues. This study explores double-sided readout—enabling improved light collection and Depth-of-Interaction (DOI) information retrieval—to mitigate this effect and enhance the timing capabilities of heterostructures. *Approach.* The time resolution and DOI performances of $3 \times 3 \times 20$ mm^3 BGO&EJ232 heterostructures were assessed in a single and double-sided readout (SSR and DSR, respectively) configuration using high-frequency electronics. *Main results.* Selective analysis of photopeak events yielded a DOI resolution of 6.4 ± 0.04 mm. Notably, the Coincidence Time Resolution (CTR) improved from 262 ± 8 ps (SSR) to 174 ± 6 ps (DSR) when measured in coincidence with a fast reference detector. Additionally, symmetrical configuration of two identical heterostructures in coincidence was tested, yielding in DSR a CTR of 254 ± 8 ps for all photopeak events and 107 ± 5 ps for the fastest events. *Significance.* By using high-frequency double-sided readout, we could measure DOI resolution and improve the time resolution of heterostructures of up to 40%. The DOI information resulted intrinsically captured in the average between the timestamps of the two SiPMs, without requiring any further correction.

1. Introduction

The challenge Time-of-Flight Positron Emission Tomography (TOF-PET) is currently facing is achieving a CTR below 100 ps while maintaining high sensitivity (Gundacker *et al* 2013, Cates and Levin 2018, Pourashraf *et al* 2021, Mariscal-Castilla *et al* 2024). Improved Signal-to-Noise Ratio (SNR) enhances image quality and diagnostic accuracy, but it also acts as a virtual sensitivity amplifier, therefore enabling lower doses for the same image quality, expanding patient eligibility, and improving workflow (Conti 2011).

Heterostructured scintillators are a possible solution to this trade-off as they consist of the combination of two or more materials with complementary properties (Lecoq 2014, Turtos *et al* 2019a, Pagano *et al* 2022a, Konstantinou *et al* 2023), i.e. high stopping power for 511 keV γ-ray and (sub-)nanosecond scintillation kinetics. The underlying principle is referred to as *energy sharing*: the 511 keV γ-ray can be fully stopped in the heavy material while the recoil photoelectron can escape from it and deposit part of its energy in the fast one. Such events are called *shared events*. This phenomenon becomes relevant when the thickness of the heavy material is comparable to the range of the recoil electron resulting from the photoelectric absorption

of a 511 keV γ-ray in the material itself (a few hundred micrometers) (Pagano *et al* 2022a). The more energy is deposited in the fast material, the more fast photons are produced, improving the overall time resolution of the detector.

The first proof-of-concept of heterostructures for TOF-PET was presented by Turtos *et al* (2019a). Here, the fast plastic scintillator BC422 (Saint-Gobain BC422 data-sheet) was successfully combined with BGO and LYSO in small ($3 \times 3 \times 3$ mm^3) pixels. This work showed the possibility of discriminating the events according to the material where the energy is deposited and gave experimental proof that this approach allows for a CTR improvement compared to the bulk, heavy material used. Further works (Lecoq *et al* 2022, Pagano *et al* 2022a, 2023, Latella *et al* 2023) investigated in more detail the properties of heterostructures with BGO or LYSO and plastic scintillators (Saint-Gobain BC422 data-sheet Eljen-technology EJ232 datasheet). These studies deepened the understanding of heterostructure properties and also tested longer heterostructure pixels (15–20 mm), reaching the length used in commercial scanners.

Although this technology is not yet a concrete alternative to LYSO (the current state of the art), due to reasons such as complex manufacturing, it has shown promising results. By choosing a material with a high photofraction, like BGO, up to half of the volume can be replaced with a fast plastic scintillator while maintaining a photoelectric probability similar to that of LYSO, and simultaneously improving the temporal performance of the heavy scintillator (Pagano *et al* 2022a). Consequently, there is significant interest in thoroughly exploring the limits of heterostructures and understanding how to address their challenges.

A particularly active area of research in the field concerns material selection, especially for the fast scintillator, which is closely related to the growing interest in nanomaterials that can potentially offer higher stopping power and photon time density than the standard plastic scintillator. A few studies have already demonstrated the applicability of these materials to heterostructures (Turtos *et al* 2019b, Orfano *et al* 2023, Rogers *et al* 2023, Pagano *et al* 2024). However, they are not without disadvantages, primarily the self-absorption (Děcká *et al* 2022, Pagano *et al* 2024) which makes it difficult to extract light in case of long pixels.

While efforts to improve the synthesis of these materials are ongoing, it is also important to keep studying the intrinsic properties of heterostructures that currently limit their performance, and BGO and EJ232 are the best candidates for this task due to their scintillation properties (Pagano *et al* 2023). One such limitation is the layering of the detector, which worsens light transport and collection, affecting by consequence its time capabilities as well. A straightforward way to increase the light collection is double-sided readout, with the added advantage of allowing for depth-of-interaction (DOI) information retrieval. As the DOI uncertainty severely biases the time of arrival distribution in long crystals, its recovery can further improve the time resolution. Moreover, at system level, especially for small scanners like the pre-clinical or organ dedicated scanners, good DOI resolution is important to correct for the parallax error (Del Guerra *et al* 2016, Gonzalez-Montoro *et al* 2022, Sanaat *et al* 2024).

With this contribution, we show how heterostructures can benefit from double side readout, or more in general from a configuration that allows for DOI estimation, using $3 \times 3 \times 20$ mm^3 BGO&EJ232 heterostructures and a custom-made high-frequency electronic circuit developed at the Lawrence Berkeley National laboratory. In section 2, the details about the heterostructure, the photosensors, and the electronics readout are described. Section 3 explains on the measurements procedure and analysis method, with a focus on different time estimators that were tested before deciding the most appropriate one. In section 4, the results are presented, starting with the comparison between single-sided readout (SSR) and double-sided readout (DSR) (section 4.1), continuing with the DOI resolution (section 4.2) and the DOI effect on timing (section 4.3), to conclude with the measurements of two heterostructures in coincidence (section 4.4), which at the best of our knowledge has never been published before and arises interesting considerations. We discuss the results in section 5 and draw the conclusion of our study in section 6.

2. Materials

2.1. Samples

For this study, two heterostructures pixels made of alternated plates of BGO and EJ232 purchased at Crystal Photonics, Inc (CPI) company were used. The overall size was $3 \times 3 \times 20$ mm^3, while the thickness of the plates was 250 μm for both materials. In our previous work, we showed that BGO&plastic heterostructure constituted by equal volume of BGO and plastic exhibit a photofraction comparable to that of LYSO (Pagano *et al* 2022a). The thickness of the layers was selected as a compromise between achieving a high probability of energy sharing and the practical considerations of cutting and handling such thin plates.

The 3×20 mm^2 surfaces of both BGO and EJ232 were polished, while the edges were left as-cut. The heterostructures were wrapped in the enhanced specular reflector (ESR). For SSR measurements, the ESR

was around both the four lateral surfaces and the opposite face to the SiPM, while in DSR around the lateral faces only.

2.2. Silicon Photomultipliers (SiPMs)

The heterostructures were coupled with Cargille Meltmount glue (refractive index $n = 1.58$) to the SiPM(s). For all the configuration tested, Broadcom NUV-HD SiPM with 3×3 mm^3 active area and 30 μm SPAD size (AFBR-S4N33C013, Broadcom NUV-HD data-sheet) were used and biased with an over voltage of about 10 V (37 V bias voltage). A subset of measurements (a detailed overview of all the configuration tested is provided in section 3) was repeated using Broadcom NUV-MT SiPMs with 3.7×3.6 mm^2 active area and 30 μm SPAD size (AFBR-S4N44P014M, Broadcom NUV-MT data-sheet), operated at a bias voltage of 47 V, corresponding to an over voltage of 15 V.

'MT' is the abbreviation for Metal-filled Trenches, a new technology developed by Fondazione Bruno Kessler (FBK) and Broadcom to suppress internal cross-talk (Merzi *et al* 2023). The microcells are surrounded by metal-filled trenches, hence they are optically isolated among each other. In such a way, the photons produced by an avalanching microcell are unlikely to travel to the neighboring microcells and initiate a secondary avalanche. The strong reduction in cross-talk allows higher bias voltages to be applied and thus higher gain and photon detection efficiency (PDE) to be achieved, ultimately leading to better timing.

2.3. Front-end readout

The front-end electronics were designed at the Lawrence Berkeley National Laboratory, based on low noise, high-frequency (HF) circuits. They consist of a balun transformer (a passive electronic component converting the unbalanced signal from the SiPM into two balanced outputs with 180° phase difference) connected between the cathode and anode of the SiPM to two radio-frequency (RF) amplifiers in cascade (Cates *et al* 2018). This circuit efficiently amplifies and extracts the high speed, high bandwidth signal from the SiPM. Because of the large voltage amplification, a second path to separately process the energy information was designed using standard AD8000 operational amplifier (Gundacker *et al* 2019).

The present electronics is analogous to the one previously described by Cates *et al* (2018) and Gundacker *et al* (2019), but designed to allow for double-sided readout of the crystal through a single printed circuit board (PCB). Moreover, the radio-frequencies (RF) amplifiers components here are Minicircuits Mar6-SM+.

The signal outputs were digitized by an 8-channel Tektronix MSO68B-400 oscilloscope, exhibiting a sampling rate of 12.5 GS s^{-1} and bandwidth of 8 GHz.

3. Method

A heterostructure was initially measured in coincidence (20 ns time window) with a reference crystal ($2 \times 2 \times 10$ mm^3 LSO:Ce:0.2% Ca, 85 ps CTR) first in single-sided readout (SSR) and next in double-sided readout (DSR), with front irradiation (i.e. irradiating the crystal face opposite to the SiPM), using a ^{22}Na source (see figures 1(a) and (b)).

The measurement in DSR was then repeated in side and collimated irradiation (i.e. irradiating the lateral face of the crystal and with electronic collimation, see figure 1(c)) to extract DOI information. To ensure the irradiation of about 2 mm spot along the heterostructure, the ^{22}Na source was placed 12 cm and 1.5 cm far from the reference crystal and the heterostructure, respectively. Eleven DOIs were irradiated to evaluate the DOI resolution of the system and perform the DOI calibration. A spacing of 1 mm was used for the critical regions, specifically at the edges and the center, while for the other regions a spacing of 2 mm was chosen. Thus, with the center of the pixel set as 0 mm, the measured DOIs were positioned at: [0, $\pm$1, $\pm$3, $\pm$5, $\pm$7, $\pm$8] mm.

Finally, the two heterostructures were measured in coincidence with each other (instead of coincident with the reference crystal). We will refer to it as symmetric configuration, and it was tested both in SSR and DSR (figures 1(d) and (e)). The measurements in symmetric configuration, as those of greatest interest for TOF-PET performance evaluation, were repeated using the NUV-MT SiPM.

In the DSR measurements, front-side and back-side refer to the 3×3 mm^2 surfaces closest and furthest away from the radioactive source, respectively. The corresponding SiPMs are referred to as front-SiPM and back-SiPM. For consistency, the same nomenclature is kept in the DOI configuration, and in the SSR configuration the readout face is referred to as back-side and the corresponding SiPM as back-SiPM.

All the necessary information for the analysis was directly extrapolated from the waveforms at the oscilloscope. Both the integrated charge and the amplitude of the energy signal were acquired to reconstruct the deposited energy in the two materials and perform an events classification as described in our previous works (Pagano *et al* 2022a, 2023). In heterostructured scintillators it is indeed possible to distinguish, among

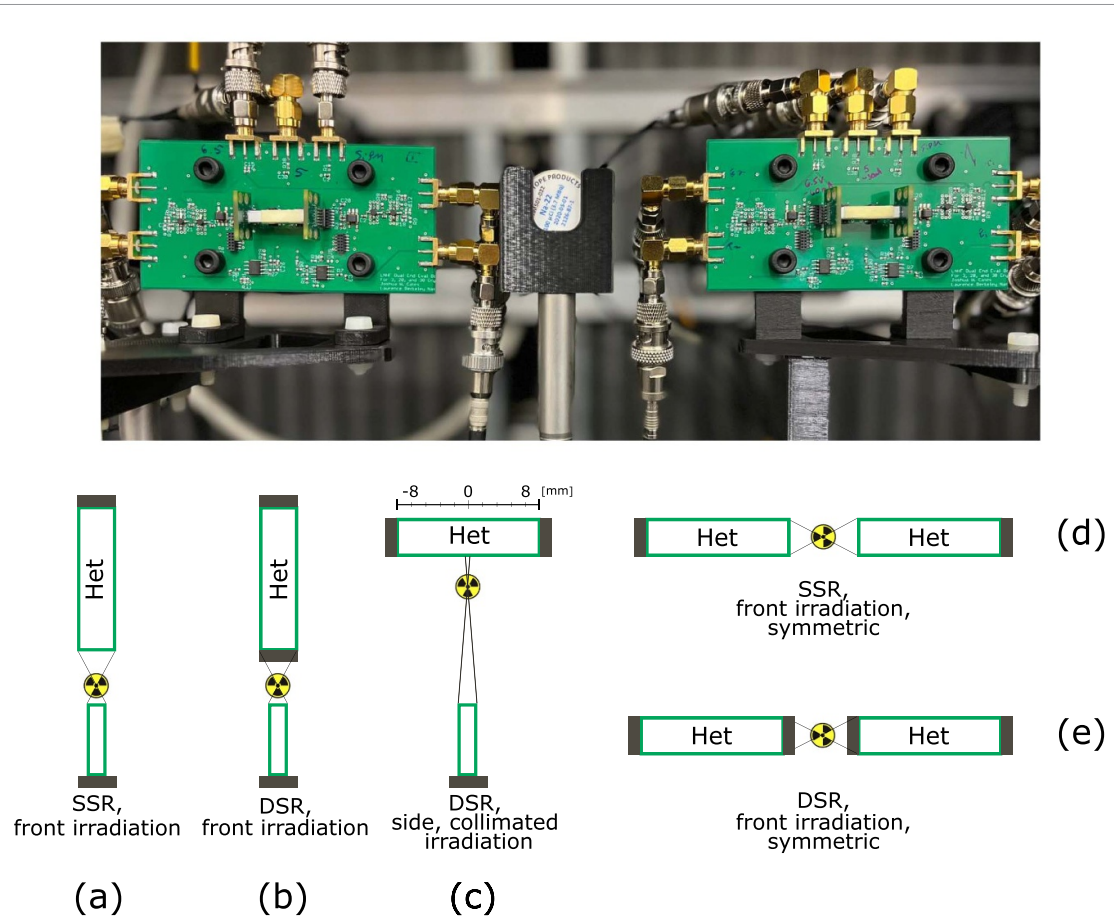

Figure 1. Top: picture of the experimental setup. Bottom: scheme of all the configuration tested; from left to right: front irradiation in single side readout (SSR) vs reference crystal, front irradiation in double side readout (DSR) vs reference crystal, side and collimated irradiation in DSR vs reference crystal, SSR of two heterostructures in coincidence with each other, DSR of two heterostructures in coincidence with each other.

photopeak events, those showing energy sharing between the two materials. Specifically, the *all photopeak events* are classified as those with a reconstructed total deposited energy between 440 keV and 665 keV. The *shared photopeak events* are selected, among these, as those with reconstructed energy deposited in plastic greater than 50 keV. The time delay between coincident detectors is recorded using the leading-edge (LED) time pick-off method, and the CTR is determined from the Full Width at Half Maximum (FWHM) of the time delay distribution. In the symmetric configuration, where two identical crystals are in coincidence, the CTR is directly given by the FWHM. When measuring in coincidence with a reference detector, the CTR is calculated by correcting the measured FWHM for the reference contribution using the formula $\mathrm{CTR_{Het}} = \sqrt{2 \cdot \mathrm{FWHM^2_{meas}} - \mathrm{CTR^2_{ref}}}$. In both cases, the FWHM was evaluated after applying the time walk correction based on the signal rise time (Kratochwil *et al* 2020, Pagano *et al* 2022a). Being the statistical error on the fit and FWHM evaluation negligible, we assessed a systematic error of 3% on the CTR during the initial validation stage of our setup and stated this finding.

3.1. Time estimators for CTR

The time delay (dt) in SSR was recorded as the time difference between the timestamps of the back SiPMs on the two sides. In DSR, the simplest time estimator is the simple average of all the time delay measured (Seifert and Schaart 2014, Kwon *et al* 2019, Weindel *et al* 2023). Equations (1)–(4) summarizes the way the time delay distribution was obtained for the different configurations, where t_{ref}, t_{back} and t_{front} refer to the timestamps of the reference detector, the back and front SiPM of the heterostructure, respectively. The subscript 1 and 2 refer to the two heterostructures in the symmetrical configuration

$$dt_{\mathrm{SSR}} = t_{\mathrm{ref}} - t_{\mathrm{back}} \tag{1}$$

$$dt_{\mathrm{DSR}} = \frac{(t_{\mathrm{ref}} - t_{\mathrm{back}}) + (t_{\mathrm{ref}} - t_{\mathrm{front}})}{2} \tag{2}$$

$$dt_{\mathrm{SSR,symm}} = t_{\mathrm{back},1} - t_{\mathrm{back},2} \tag{3}$$

$$dt_{\mathrm{DSR,symm}} = \frac{(t_{\mathrm{back},1} - t_{\mathrm{back},2}) + (t_{\mathrm{front},1} - t_{\mathrm{front},2})}{2}. \tag{4}$$

Although the simple average is the simplest estimator one can choose, it is not necessarily the most accurate. We also tested the covariance combination and two different weighted averages, which we are now going to explain in more detail.

Because a correlation between the timestamps measured by the back- and front-SiPM could exist, we evaluated the covariance elements (equation (5)) and the correlation coefficient (equation (6)). In case of significant correlation, the covariance combination (equation (8)) should be used instead of the simple average

$$\sigma_{\mathrm{f,b}} = \frac{1}{N} \cdot \sum_{i}^{N} \left(t_{\mathrm{b},i} - \hat{t_{\mathrm{b}}}\right) \cdot \left(t_{\mathrm{f},i} - \hat{t_{\mathrm{f}}}\right) \tag{5}$$

$$r = \sigma_{\mathrm{f,b}} / \left(\sigma_{\mathrm{f}} \cdot \sigma_{\mathrm{b}}\right) \tag{6}$$

$$w_{\mathrm{b}} = \frac{\sigma_f^2 - \sigma_{\mathrm{f,b}}}{\sigma_{\mathrm{f}}^2 + \sigma_{\mathrm{b}}^2 - 2 \cdot \sigma_{\mathrm{f,b}}}, \qquad w_{\mathrm{f}} = \frac{\sigma_{\mathrm{b}}^2 - \sigma_{\mathrm{f,b}}}{\sigma_{\mathrm{f}}^2 + \sigma_{\mathrm{b}}^2 - 2 \cdot \sigma_{\mathrm{f,b}}} \tag{7}$$

$$dt_{\mathrm{DSR},c} = t_{\mathrm{b}} \cdot w_{\mathrm{b}} + t_{\mathrm{f}} \cdot w_{\mathrm{f}}. \tag{8}$$

As time resolution scales as the inverse of the number of detected photons squared root (Sigfridsson 1967, Vinogradov 2018, Gundacker *et al* 2020, Pagano *et al* 2022b), a weighted average of the timestamps using as weighting factors the charge collected by the corresponding SiPMs ($IntCh_{\mathrm{b/f}}$) was also tested:

$$dt_{\mathrm{DSR},w1} = \frac{t_{\mathrm{b}} \cdot IntCh_{\mathrm{b}} + t_{\mathrm{f}} \cdot IntCh_{\mathrm{f}}}{IntCh_{\mathrm{b}} + IntCh_{\mathrm{f}}}. \tag{9}$$

Finally, due to the direction of propagation of the γ-ray, the time resolution measured by the front- and back-SiPM is not the same. In particular, the DOI contribution is higher for the front-SiPM, resulting in a worse temporal resolution for the latter. The weighted average using the standard deviation (σ_{b} and σ_{f}) of the two timestamps as a weighting factor was therefore evaluated:

$$dt_{\mathrm{DSR},w2} = \frac{t_{\mathrm{b}}/\sigma_{\mathrm{b}}^2 + t_{\mathrm{f}}/\sigma_{\mathrm{f}}^2}{1/\sigma_{\mathrm{b}}^2 + 1/\sigma_{\mathrm{f}}^2}. \tag{10}$$

3.2. DOI resolution

The estimator used for the DOI coordinate was the contrast c between the integrated charge collected by the back and front SiPM (Salvador *et al* 2010, Seifert and Schaart 2014):

$$c = \frac{IntCh_{\mathrm{b}} - IntCh_{\mathrm{f}}}{IntCh_{\mathrm{b}} + IntCh_{\mathrm{f}}}. \tag{11}$$

For each DOI measurement, the contrast c was computed on event-basis and the resulting distributions were fitted with a Gaussian function. The mean of the Gaussian was then correlated to the nominal DOI position, and the resulting calibration curve was used to reconstruct the DOI in millimeters. For each event, the difference between the nominal and the reconstructed DOI was computed and the FWHM of the resulting distribution was stated as DOI resolution of our detector unit (Pizzichemi *et al* 2016). This procedure was performed both by merging all the data and for each irradiation position individually, in order to have the overall DOI resolution of the pixel and to study any dependence of the resolution with the DOI position itself. The reported DOI resolution does not take into account the physical size of the beam spot (about 2 mm), because, given the results and assuming that both the intrinsic DOI resolution and the beam spot are Gaussian contributions, the intrinsic DOI resolution is comparable to the measured FWHM ($DOI_{\mathrm{intr}} = \sqrt{\mathrm{FWHM}^2 - (\mathrm{spot\,size})^2}$.

The analysis was performed both for *all photopeak events* and distinguishing them between only *BGO* (energy deposited in EJ232 less than 50 keV) and only *shared photopeak events* (energy deposited in EJ232 more than 50 keV) separately.

3.3. DOI-based time correction

Previous works (Pizzichemi *et al* 2019) showed how the DOI information can be used to improve the time resolution. Therefore, the correlation between the center of the time delay peak with the DOI coordinate estimator was also studied and the resulting calibration curve was then used to correct the timestamps in similar way to that used to reconstruct the interaction position. This procedure was done separately for the timestamps of back and front SiPMs, which were subsequently combined as described in section 3.1.

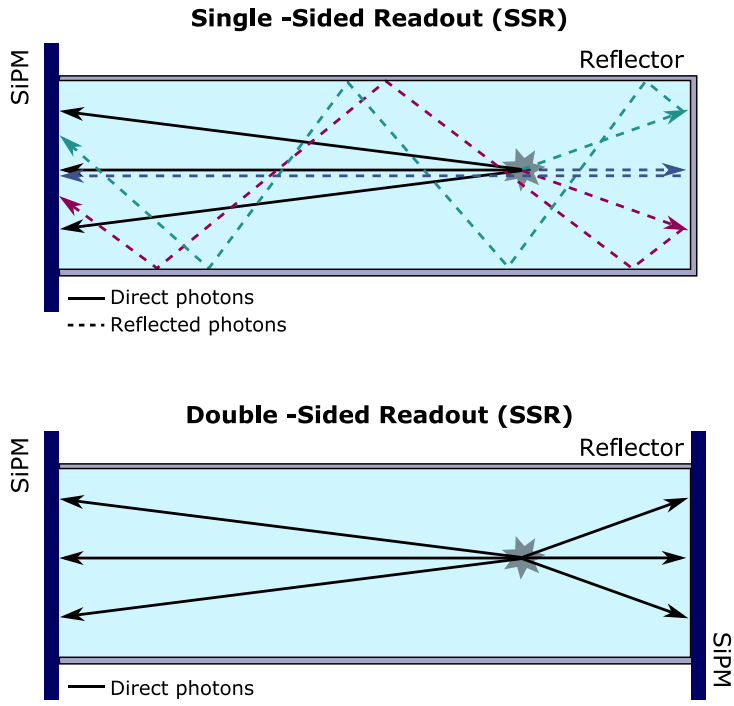

Figure 2. Sketch of the path traveled by the detected optical photons in single- and double-sided readout.

4. Results

4.1. Single vs double-ended readout

The first advantage of DSR is the increased light collection. In crystals with high aspect ratio, the first photons reaching the SiPM are those emitted along the two longitudinal directions. While in SSR the photons emitted toward the opposite face to the SiPM have high probability to be absorbed, in DSR a large part of these photons is not reflected back but directly detected, as shown in the sketch in figure 2.

Figure 3 (a) shows the comparison between the integrated charge in SSR and DSR, where one can observe the shift of the 511 keV photopeak from 4.06 a.u. (SSR) to 5.77 a.u. (DSR).

As the CTR scales as the inverse of the square root of the light output (Sigfridsson 1967), considering the shift of the photopeak in the integrated charge distribution we expected a CTR improvement of at least 15% due to this effect. The CTR in SSR for *all the photopeak events* resulted in 262 ± 8 ps, while selecting only the *shared photopeak events* (constituting the 30% of all the photopeak events) 205 ± 6 ps were measured. In DSR, by using the simple average between the timestamps of back and front SiPM (equation (1)), CTR of 174 ± 6 ps and 117 ± 5 ps were obtained for all and only *shared photopeak events*, respectively. Figures 3(b) and (c) show the comparison of the time delay distribution between single and double sided readout for all the photopeak events and for only shared ones, respectively.

The timing improvement when moving from SSR to DSR is therefore 34% for *all* photopeak events and 42% for only *shared photopeak events*, which exceeds the one predicted considering only the larger light output in DSR compared to SSR.

No further improvement was registered when using the other time estimators described in section 3 (equations (8)–(10)). Also, a correlation factor (equation (6)) of 0.006 was found, suggesting that the back and front timestamp are not correlated.

4.2. DOI resolution

Figure 4 (a) shows for each DOI the correlation between the integrated charge of front and back SiPMs. For each measured DOI, the contrast c (equation (11)) was evaluated and the correlation with the nominal DOI coordinate was studied, as shown in figures 4(b) and (c). Here, one might notice that the contrast measured for the central DOI (0 mm) is not zero as expected. We assessed that this was caused by a small difference in the gain of the two SiPMs and that it does not affect the results: by normalizing the charge collected for the two SiPMs individually, the asymmetry was suppressed and the DOI resolution was the same. The contrast c was found to be linear with the nominal DOI, therefore the calibration curve used to extract the DOI

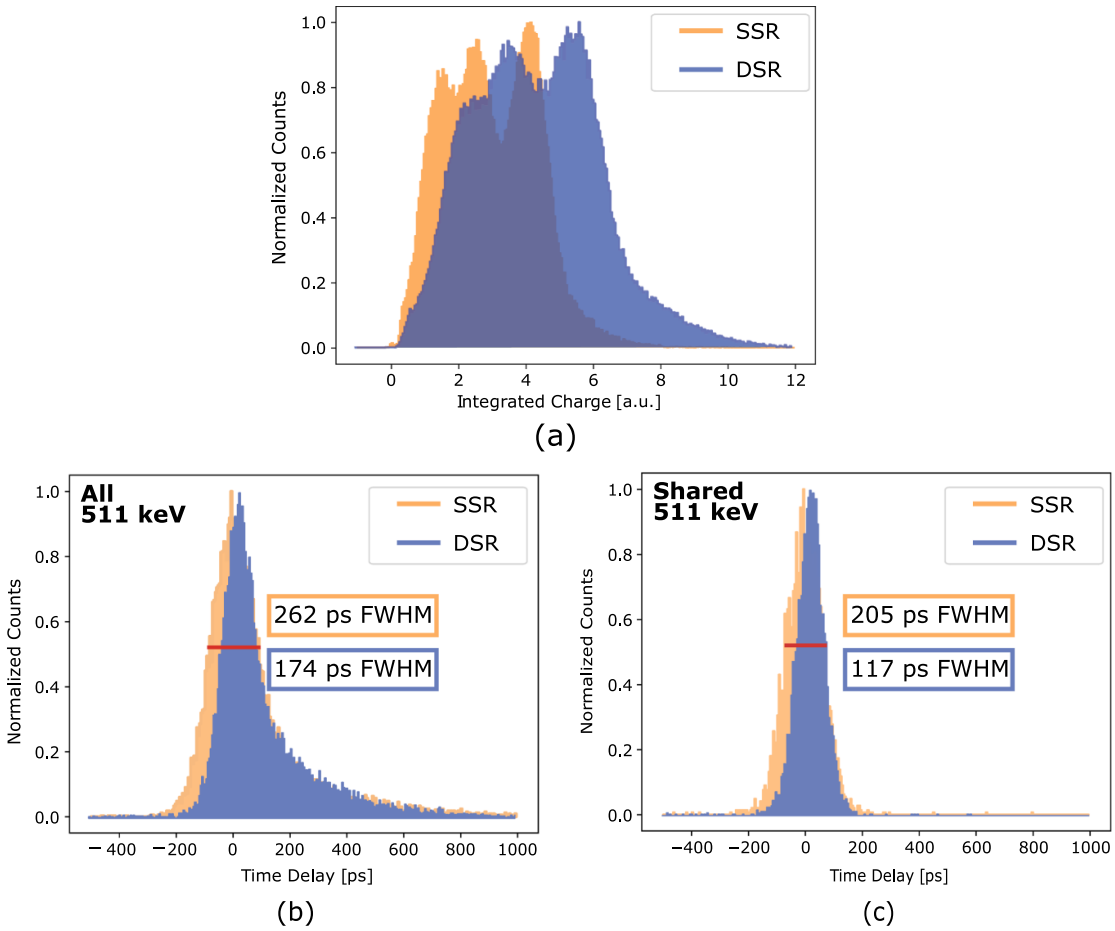

Figure 3. Comparison between single-sided readout (SSR) and double-sided readout (DSR) of (a) integrated charge in the two configurations, (b) time delay distribution of *all photopeak events* and of (c) only *shared photopeak events*.

resolution of the pixel was simply given by

$$\mathrm{DOI}_{\mathrm{coord}} = m \cdot c + q, \tag{12}$$

with m and q being the slope and intercept of the fit curve.

A DOI resolution ranging between 5.86 ± 0.04 mm and 7.47 ± 0.04 mm, with a variance of 0.5 mm was measured for the individual DOI measurements. By merging all the data, a overall DOI resolution of 6.40 ± 0.04 mm FWHM was obtained. These results refer to the *all photopeak events* while, by distinguishing between only *BGO photopeak events* and only *shared photopeak events*, we got a DOI resolution of 7.0 ± 0.5 mm and 5.7 ± 0.5 mm, respectively.

4.3. DOI-based time correction

A linear dependence of the time delay peak on the DOI coordinate for the back and front SiPM taken individually was found (see figure 5). Similarly as before, for each event the contrast c was computed together with the corrective factor, given by

$$dt_{\mathrm{corr}} = m_t \cdot c + q_t, \tag{13}$$

with m_t and q_t being the slope and intercept of the fit curves. The correction was then performed by subtracting to each timestamps the corresponding corrective factor.

Table 1 summarizes the CTR results in front irradiation in SSR and DSR configuration, without and with DOI correction. It can be seen the DOI-based time correction does not bring any further improvement compared to the simple average of the back and front timestamps. This result is consistent with what is shown in figure 5: the time delay peaks from the two individual SiPMs move linearly with the DOI estimator c, in equal but opposite direction, but the simple average shows no dependence on the DOI coordinate. The simple average alone is therefore enough to suppress the DOI contribution to time resolution.

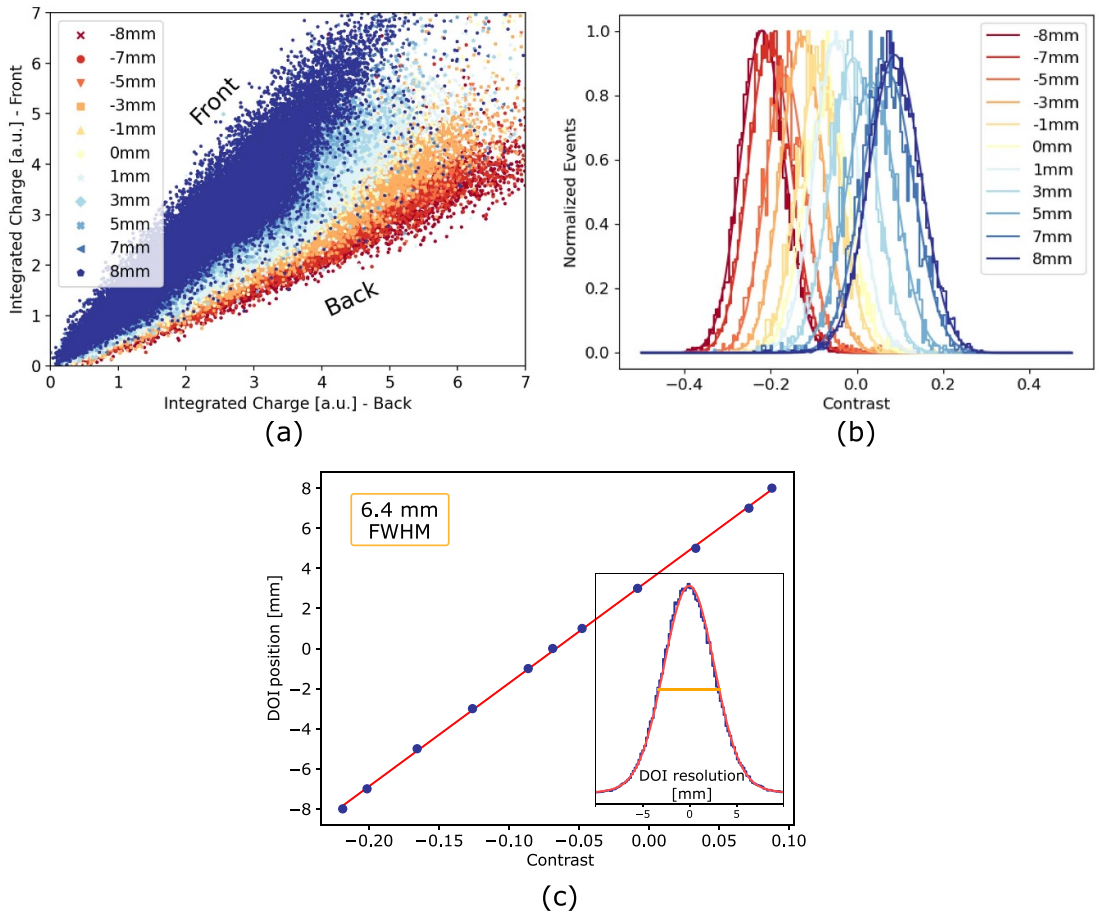

Figure 4. DOI calibration. (a) Correlation between the integrated charge collected by the two side according to the DOI. (b) Contrast between the two SiPMs on the opposite sides. (c) DOI calibration curve and DOI resolution.

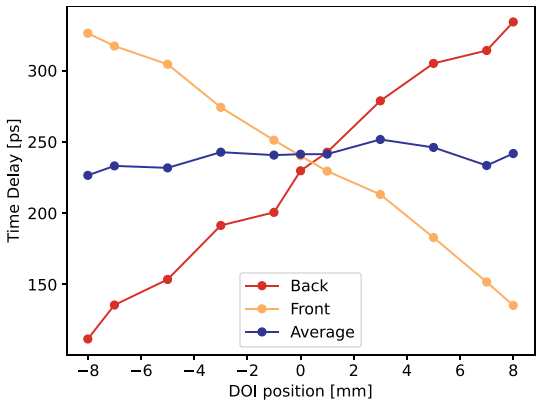

Figure 5. Correlation between time delay and DOI coordinate. This is shown both for the front and back SiPM individually and for the average of the timestamp.

4.4. Symmetric configuration

The results showed until now refer to heterostructured pixels measured in coincidence with a (fast) reference crystal. This configuration is widely used to reduce systematics and accurately characterize the sample under investigation. However, it does not always provide an accurate prediction of the real timing performance of the detector of interest. The main reason for this lies in the method used to correct the contribution of the reference detector. By using quadratic subtraction and multiplying by $\sqrt{2}$, we are assuming the timestamps to be distributed according to a single Gaussian. This assumption is not valid for heterostructures made of materials characterized by light emission processes with strongly different timescales. Indeed, each event with a given ratio of energy deposited in BGO and EJ232, gives rise to a different CTR distribution.

Table 1. CTR results in SSR and DSR using NUV-HD SiPMs. The results are presented distinguishing between *all* and only *shared photopeak events*. The results in DSR after applying the correction for DOI are also reported (DSR + DOI corr).

Events type	SSR (ps)	DSR (ps)	DSR + DOI corr (ps)
All Photopeak	262 ± 8	174 ± 6	174 ± 6
Shared Photopeak	205 ± 6	117 ± 5	123 ± 5

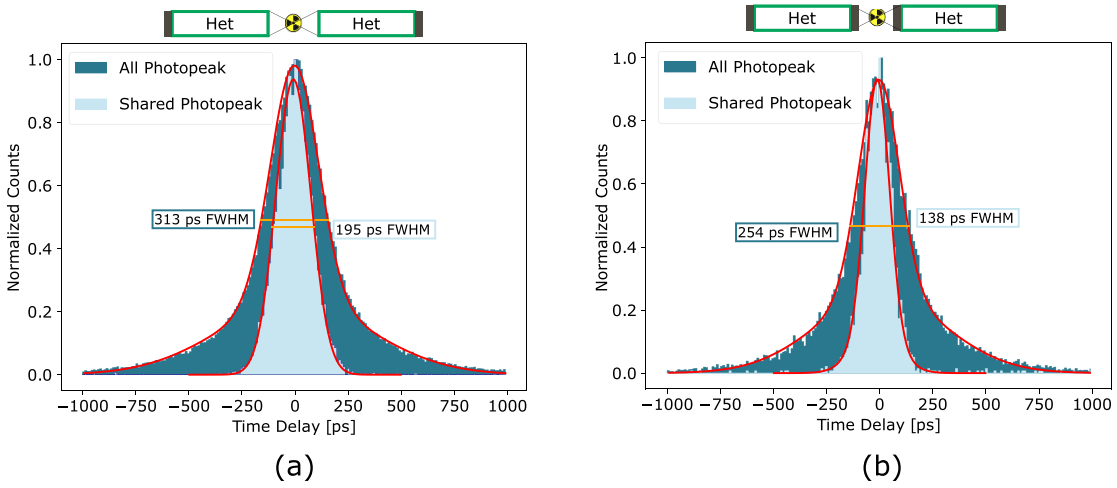

Figure 6. CTR in single-sided readout (a) and double-sided readout (b) for all photopeak events and only *shared photopeak events*, in symmetrical configuration.

Table 2. Comparison of CTR results in SSR and DSR when measuring in coincidence with a reference detector or in symmetric configuration, using NUV-HD SiPM.

Events type	SSR (vs reference) (ps)	SSR (symm.) (ps)	DSR (vs reference) (ps)	DSR (symm.) (ps)
All Photopeak	262 ± 8	313 ± 9	174 ± 6	254 ± 8
Shared Photopeak	205 ± 6	195 ± 6	117 ± 5	138 ± 5

Therefore, we measured also two identical heterostructures in coincidence, both in SSR and DSR. Figure 6 shows the time delay distribution obtained in the two configurations, distinguishing between *all* and only *shared photopeak events*. The resulting CTR values are shown in table 2, in comparison with those obtained measuring in coincidence with a reference detector. When considering *all photopeak events*, the measured CTR in symmetric configuration is significantly worse. Such CTR degradation is not observed when selecting photopeak events which are *shared photopeak events* in both heterostructures simultaneously.

To gain a better understanding of the CTR distribution in heterostructures, photopeak events were categorized based on the amount of energy deposited in EJ232. Three energy intervals were selected for each detector: 0–50 keV, 50–250 keV, and 250–500 keV. All possible combinations of these energy intervals in both detectors were considered (Kratochwil *et al* 2020). Figure 7 summarizes the CTR measured for all the potential combinations considered is SSR (left) and DSR (right).

In SSR, the CTR of all photopeak events is 313 ± 9 ps and 195 ± 6 ps for only *shared photopeak events*. When considering only the BGO photopeak events on both detector sides, the CTR increases up to 394 ± 11 ps, while if we select only the fastest events (i.e. those with more than 250 keV deposited in EJ232 on both sides, corresponding only to the 1% of the photopeak events) it improves up to 181 ± 6 ps.

Repeating the same exercise for the DSR configuration, 254 ± 8 ps CTR was measured for all photopeak events and 138 ± 5 ps for only *shared photopeak events* (50% of the all photopeak events). In the two extreme cases, a CTR of 386 ± 11 ps was measured for only BGO photopeak events of both sides and of 107 ± 5 ps for the fastest 1% of the events.

The same measurements, i.e. two identical heterostructures in coincidence both in SSR and DSR, were repeated using the NUV-MT SiPMs, which are expected to provide better results due to the strong suppression of internal cross-talk (Merzi *et al* 2023). The results are shown in table 3, in comparison with the results previously obtained with the NUV-HD SiPMs.

The CTR improvement in SSR is remarkable especially when considering *all photopeak events*, i.e. where there is an important contribution from BGO: from 313 ± 9 ps (NUV-HD) to 270 ± 8 ps (NUV-MT).

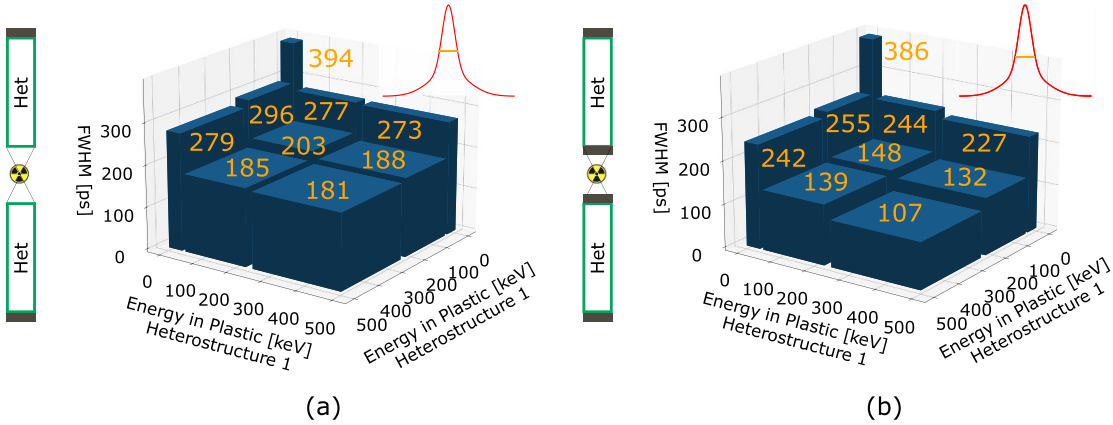

Figure 7. Measured CTR in SSR (a) with NUV-HD SiPM and DSR (b) for all the potential combination of events considered.

Table 3. CTR results in SSR and DSR comparing Broadcom SiPM belonging to NUV-HD and NUV-MT technology, in symmetric configuration.

	CTR (ps) SSR		CTR (ps) DSR	
Events type	NUV-HD	NUV-MT	NUV-HD	NUV-MT
All Photopeak	313 ± 9	270 ± 8	254 ± 8	239 ± 8
Shared Photopeak	195 ± 6	181 ± 6	138 ± 5	136 ± 5

Surprisingly, considering the overlap of the error intervals, no improvement was observed in DSR when switching from NUV-HD to NUV-MT technology: from 254 ± 8 ps (NUV-HD) to 239 ± 8 ps (NUV-MT).

5. Discussion and outlook

Double-sided readout allows in first instance for an increased light collection compared to the single-sided readout configuration. This effect alone already improves the time resolution of the detector, because of the inverse proportionality relation between time resolution and the square root of the light output (Sigfridsson 1967). The estimated CTR improvement according to the registered light output increase was of 15%. However, when measuring in DSR and averaging the front and back timestamps, a CTR improvement between 35% and 40% was achieved compared to SSR. Such improvement occurs because DSR also allows to mitigate the time bias induced by the different DOIs of the incoming γ-ray. Due to the attenuation of the optical photons along the crystal, the back and front SiPM will detect a different amount of photons depending on the interaction position and this asymmetry allows to retrieve the DOI information.

The time bias due to the DOI uncertainty is larger in layered pixels like heterostuctures compared to bulk crystal (Pagano *et al* 2022a). Therefore, it is even more crucial to correct for this bias in heterostructures. A recent study applying DSR (also using HF electronics) to 20 mm long LYSO fibers reported an improvement between 10% and 13% (Weindel *et al* 2023).

From our results, in DSR, the simple average of the two timestamps is enough to compensate for the DOI effect, without the need of any further correction. More refined time estimators have also been tested, but they did not lead to further improvement. Among these we tested the covariance combination but a correlation factor of only 0.006 was found, leading us to conclude that the timestamps measured by the back and front SiPMs are not correlated. We explained this as an effect of light transport: although the length of the crystal is fixed and one might expect a clear correlation between the two measured timestamps, photons are emitted isotropically, can undergo different reflections and the resulting photon time spread causes correlation to be lost. This effect is further enhanced in heterostructures by the layered structure.

Regarding the DOI capability, for a single heterostructure pixel a resolution of 6.40 ± 0.04 was obtained. Assuming that the resolution does not get worse once the detector unit is integrated in a full system, it would allow three regions to be distinguished along the crystal, making parallax error correction possible.

A more in-depth analysis of DOI resolution allowed to establish that this is superior for events depositing energy also in EJ232. This can be attributed to the higher attenuation of EJ232 compared to BGO, because of its partial self-absorption generating a greater asymmetry in the amount of detected photons between the two SiPMs. Such asymmetry is the reason why with bulk crystals a superior DOI resolution is obtained with

depolished crystals (Trummer *et al* 2009, Seifert and Schaart 2014, Pizzichemi *et al* 2016, 2019). This information could be used for a more accurate parallax error correction in a full integrated system and/or a more accurate DOI-based time correction in SSR configuration where the light re-circulation and light sharing method are implemented (Pizzichemi *et al* 2019).

Despite the important performance advantages that can be achieved with DSR, to date it is not a cost-effective solution as it requires doubling the readout channels. However, while work is being done to make this technology more practical (both economically and geometrically), this study provides promising results on the implementation of a heterostructure array, with readout in a single-sided configuration in which the light-sharing method is applied to retrieve DOI information (Pizzichemi *et al* 2019).

This work also highlights the complexity of the CTR distribution when measuring two heterostructures in coincidence because of all the possible combinations of different event types (shared events in only one, both or none detector arm and how much energy is shared) in the two detectors. With the described events classification, we were able to obtain 181 ps (SSR) and 107 ps (DSR) for the fastest event class. These values, even if they refer to 1% of the events, significantly differ from the average CTR obtained when merging all the events (313 ps in DSR and 254 ps). These results suggest that, in the reconstruction process, a unique value to describe the CTR of a heterostructure module could not be accurate. As already proposed (Efthimiou *et al* 2020, Mohr *et al* 2022), a multi-kernel approach, accounting for different CTR depending on the event type, could represent a more appropriate solution. This approach needs further investigation and the key aspects to be considered include the percentage of the fastest events and the corresponding CTR required to achieve a meaningful improvement in image quality. The outcomes of this study could also guide the development of the next generation of heterostructures by setting critical requirements for timing, sensitivity, and energy-sharing fractions.

Finally, the measurements in symmetric configuration were repeated using the NUV-MT SiPM from Broadcom, expected to provide even better timing because of the internal cross-talk suppression (Merzi *et al* 2023), which allows to reach larger gain and PDE. Ultimately, for a 20 mm long heterostructure, when considering all the photopeak events, CTR of 270 ± 8 ps and 239 ± 8 ps where measured in SSR and DSR, respectively. By selecting only the *shared photopeak events*, these values improves up to 181 ± 6 ps (SSR) and 136 ± 5 ps (DSR).

Looking at table 3, one can observe that in DSR configuration no improvement is recorded when transitioning from NUV-HD to NUV-MT SiPM. This was unexpected due to the larger PDE and more favorable active area (3.7×3.6 mm^2 for a 3×3 mm^2 pixel cross section) of the MT SiPM. One possible explanation is that while MT technology suppresses internal crosstalk, external crosstalk is still present and its contribution is more important in DSR than SSR configuration. Therefore, while MT SiPMs allow unprecedented over voltages to be achieved without being affected by internal crosstalk, the probability of external crosstalk increases. In SSR, secondary photons (i.e. photons produced by an avalanching microcell which are able to escape the SiPM surface) are anyway likely to be absorbed, as they would need to travel twice the length of the pixel, whereas in DSR the probability of them being detected by the second SiPM becomes significant. This hypothesis will need further testing and investigation to be confirmed or not, and new measurements with bulk BGO and EJ232 pixels are already underway.

6. Conclusion

In this work, we measured $3 \times 3 \times 20$ mm^3 BGO&EJ232 heterostructure using both single-sided (SSR) and double-sided (DSR) readout configurations. First, one heterostructures was measured in coincidence against a fast reference detector, to better investigate the achievable improvement when transitioning from SSR to DSR and to accurately extract the DOI information. CTR values of 262 ± 8 ps (SSR) and 174 ± 6 ps (DSR) were measured when considering *all the photopeak events*, while 205 ± 6 (SSR) and 117 ± 5 ps (DSR) CTR were obtained for only *shared photopeak events*.

A DOI resolution of 6.40 ± 0.04 mm was measured for the detector under test. Assuming that similar resolution is also maintained when integrating this detector into a complete system, three regions could be distinguished along the crystal (being 20 mm long) and allow parallax error correction. This information was not used to further improve the timing performances of the heterostructure, as the simple average of the timestamps resulted enough to compensate for the DOI effect.

When measuring two heterostructures in coincidence, using the state-of-the-art NUV-MT Broadcom SiPM, CTR values of 239 ± 8 ps (*all photopeak events*) and 136 ± 5 ps (*shared photopeak events*) were achieved in DSR. This configuration also highlighted the complex CTR distribution in heterostructure which can be used as input in the image reconstruction process based on multi-kernel approach.

Overall, this study shows the enormous improvement that can be achieved in the timing performance of heterostructured scintillators with DSR. Although DSR is not an affordable system-level solution to date, it

provides valuable insights into the performance of the TOF-PET modules made of heterostructures in SSR, where other techniques can be used to extract DOI information and to correct both timing and parallax error.

Data availability statement

The data cannot be made publicly available upon publication because they are not available in a format that is sufficiently accessible or reusable by other researchers. The data that support the findings of this study are available upon reasonable request from the authors.

Acknowledgments

This work was carried out in the frame of the Crystal Clear Collaboration. It received support from the CERN Budget for Knowledge Transfer to Medical Applications and from the Wolfgang Gentner Programme of the German Federal Ministry of Education and Research (Grant No. 13E18CHA). Some material was based upon work supported by the National Institutes of Health under research Grant R01EB028286. The authors would like to thank Isabel Frank for her help in the preparation of the mechanics for the experimental setup.

ORCID iDs

Fiammetta Pagano https://orcid.org/0000-0001-9938-6799
Nicolaus Kratochwil https://orcid.org/0000-0001-5297-1878
Carsten Lowis https://orcid.org/0000-0002-7194-3917
Marco Pizzichemi https://orcid.org/0000-0001-5189-230X
Joshua W Cates https://orcid.org/0000-0002-5649-8691
Etiennette Auffray https://orcid.org/0000-0001-8540-1097

References

Broadcom NUV-HD (data-sheet) Broadcom NUV-HD silicon photomultiplier 3.14 × 3.14 active area (available at: www.broadcom.com/products/optical-sensors/silicon-photomultiplier-sipm/afbr-s4n33c013)
Broadcom NUV-MT (data-sheet) Broadcom NUV-MT silicon photomultiplier 3.7 × 3.6 active area (available at: www.broadcom.com/products/optical-sensors/silicon-photomultiplier-sipm/high-performance-sipm-nuv-mt/afbr-s4n44p014m)
Cates J W, Gundacker S, Auffray E, Lecoq P and Levin C S 2018 Improved single photon time resolution for analog SiPMs with front end readout that reduces influence of electronic noise *Phys. Med. Biol.* **63** 185022
Cates J W and Levin C S 2018 Evaluation of a clinical TOF-PET detector design that achieves ⩽100 ps coincidence time resolution *Phys. Med. Biol.* **63** 115011
Conti M 2011 Focus on time-of-flight PET: the benefits of improved time resolution *Eur. J. Nucl. Med. Mol. Imaging* **38** 1147–57
Děcká K, Pagano F, Frank I, Kratochwil N, Mihóková E, Auffray E and Čuba V 2022 Timing performance of lead halide perovskite nanoscintillators embedded in a polystyrene matrix *J. Mater. Chem.* **10** 12836–43
Del Guerra A, Belcari N and Bisogni M 2016 Positron emission tomography: its 65 years *Riv. Nuovo Cim.* **39** 155–223
Efthimiou N, Kratochwil N, Gundacker S, Polesel A, Salomoni M, Auffray E and Pizzichemi M 2020 TOF-PET image reconstruction with multiple timing kernels applied on Cherenkov radiation in BGO *IEEE Trans. Radiat. Plasma Med. Sci.* **5** 703–11
Eljen-technology (EJ232 datasheet) EJ232 datasheet (available at: https://eljentechnology.com/products/plastic-scintillators/ej-2 32-ej-232q)
Gonzalez-Montoro A *et al* 2022 A new brain dedicated PET scanner with 4D detector information *Bio-Algorithms Med-Syst.* **18** 107–19
Gundacker S, Auffray E, Frisch B, Jarron P, Knapitsch A, Meyer T, Pizzichemi M and Lecoq P 2013 Time of flight positron emission tomography towards 100ps resolution with L(Y)SO: an experimental and theoretical analysis *J. Instrum.* **8** 07014
Gundacker S, Turtos R M, Auffray E, Paganoni M and Lecoq P 2019 High-frequency SiPM readout advances measured coincidence time resolution limits in TOF-PET *Phys. Med. Biol.* **64** 055012
Gundacker S, Turtos R M, Kratochwil N, Pots R-H, Paganoni M, Lecoq P and Auffray E 2020 Experimental time resolution limits of modern SiPMs and TOF-PET detectors exploring different scintillators and Cherenkov emission *Phys. Med. Biol.* **65** 025001
Konstantinou G, Latella R, Moliner L, Zhang L, Benlloch J, Gonzalez A and Lecoq P 2023 A proof-of-concept of cross-luminescent metascintillators: testing results on a BGO:BaF_2 metapixel *Phys. Med. Biol.* **68** 025018
Kratochwil N, Gundacker S, Lecoq P and Auffray E 2020 Pushing cherenkov PET with BGO via coincidence time resolution classification and correction *Phys. Med. Biol.* **65** 115004
Kwon S I, Roncali E, Gola A, Paternoster G, Piemonte C and Cherry S R 2019 Dual-ended readout of bismuth germanate to improve timing resolution in time-of-flight PET *Phys. Med. Biol.* **64** 105007
Latella R, Gonzalez A J, Bonifacio D A, Kovylina M, Griol A, Benlloch J M, Lecoq P and Konstantinou G 2023 Exploiting Cherenkov radiation with BGO-based metascintillators *IEEE Trans. Radiat. Plasma Med. Sci.* **7** 810–8
Lecoq P P 2014 ERC advanced grant TICAL 338953 (available at: https://cordis.europa.eu/project/id/3389 53)
Lecoq P, Konstantinou G, Latella R, Moliner L, Nuyts J, Zhang L, Barrio J, Benlloch J and Gonzalez A 2022 Metascintillators: new results for TOF-PET applications *IEEE Trans. Radiat. Plasma Med. Sci.* **6** 510–6
Mariscal-Castilla A *et al* 2024 Toward sub-100 ps TOF-PET systems employing the fastic ASIC with analog SiPMs *IEEE Trans. Radiat. Plasma Med. Sci.* **8** 718–33
Merzi S, Brunner S E, Gola A, Inglese A, Mazzi A, Paternoster G, Penna M, Piemonte C and Ruzzarin M 2023 NUV-HD SiPMs with metal-filled trenches *J. Instrum.* **18** 05040

Mohr P, Efthimiou N, Pagano F, Kratochwil N, Pizzichemi M, Tsoumpas C, Auffray E and Ziemons K 2022 Image reconstruction analysis for positron emission tomography with heterostructured scintillators *IEEE Trans. Radiat. Plasma Med. Sci.* **7** 41–51

Orfano M *et al* 2023 Fast emitting nanocomposites for high-resolution TOF-PET imaging based on multicomponent scintillators *Adv. Mater. Technol.* **9** 2302075

Pagano F, Král J, Děcká K, Pizzichemi M, Mihóková E, Čuba V, Auffray E 2024 Nanocrystalline lead halide perovskites to boost time-of-flight performance of medical imaging detectors *Adv. Mater. Interfaces* **11** 2300659

Pagano F, Kratochwil N, Frank I, Gundacker S, Paganoni M, Pizzichemi M, Salomoni M and Auffray E 2022b A new method to characterize low stopping power and ultra-fast scintillators using pulsed x-rays *Front. Phys.* **10** 1021787

Pagano F, Kratochwil N, Martinazzoli L, Lowis C, Paganoni M, Pizzichemi M and Auffray E 2023 Modeling scintillation kinetics and coincidence time resolution in heterostructured scintillators *IEEE Trans. Nucl. Sci.* **70** 2630–37

Pagano F, Kratochwil N, Salomoni M, Pizzichemi M, Paganoni M and Auffray E 2022a Advances in heterostructured scintillators: toward a new generation of detectors for TOF-PET *Phys. Med. Biol.* **67** 135010

Pizzichemi M, Polesel A, Stringhini G, Gundacker S, Lecoq P, Tavernier S, Paganoni M and Auffray E 2019 On light sharing TOF-PET modules with depth of interaction and 157 ps FWHM coincidence time resolution *Phys. Med. Biol.* **64** 155008

Pizzichemi M, Stringhini G, Niknejad T, Liu Z, Lecoq P, Tavernier S, Varela J, Paganoni M and Auffray E 2016 A new method for depth of interaction determination in PET detectors *Phys. Med. Biol.* **61** 4679

Pourashraf S, Gonzalez-Montoro A, Won J Y, Lee M S, Cates J W, Zhao Z, Lee J S and Levin C S 2021 Scalable electronic readout design for a 100 ps coincidence time resolution TOF-PET system *Phys. Med. Biol.* **66** 085005

Rogers E, Birowosuto M D, Maddalena F, Dujardin C, Pagano F, Kratochwil N, Auffray E, Krause P and Bizarri G 2023 Two-dimensional perovskite functionalized fiber-type heterostructured scintillators *Appl. Phys. Lett.* **122** 081901

Saint-Gobain (BC422 data-sheet) BC422 data-sheet (available at: www.crystals.saint-gobain.com/radiation-detection-scintillators/plastic-scintillators/fast-timing-bc-418-bc-420-bc-422-bc-422q)

Salvador S, Wurtz J and Brasse D 2010 Optimizing PET DOI resolution with crystal coating and length *IEEE Trans. Nucl. Sci.* **57** 2468–74

Sanaat A, Amini M, Arabi H and Zaidi H 2024 The quest for multifunctional and dedicated PET instrumentation with irregular geometries *Ann. Nucl. Med.* **38** 31–70

Seifert S and Schaart D R 2014 Improving the time resolution of TOF-PET detectors by double-sided readout *IEEE Trans. Nucl. Sci.* **62** 3–11

Sigfridsson B 1967 Theoretical analysis of time resolution in scintillation detectors *Nucl. Instrum. Methods* **54** 13–28

Trummer J, Auffray E and Lecoq P 2009 Depth of interaction resolution of luAP and LYSO crystals *Nucl. Instrum. Methods Phys. Res.* A **599** 264–9

Turtos R M, Gundacker S, Auffray E and Lecoq P 2019a Towards a metamaterial approach for fast timing in PET: experimental proof-of-concept *Phys. Med. Biol.* **64** 185018

Turtos R *et al* 2019b On the use of CdSe scintillating nanoplatelets as time taggers for high-energy gamma detection *npj 2D Mater. Appl.* **3** 37

Vinogradov S 2018 Approximations of coincidence time resolution models of scintillator detectors with leading edge discriminator *Nucl. Instrum. Methods Phys. Res.* A **912** 149–53

Weindel K, Nadig V, Herweg K, Schulz V and Gundacker S 2023 A time-based double-sided readout concept of 100 mm LYSO:Ce,Ca fibres for future axial TOF-PET *EJNMMI Phys.* **10** 43